

# Optimization and development of a universal flow-based microfluidic gradient generator

Zhongbin Xu<sup>1,2</sup> · Xing Huang<sup>1</sup> · Pengfei Wang<sup>1</sup> · Huanan Wang<sup>2,3</sup> · David A. Weitz<sup>2</sup>

Received: 12 January 2016 / Accepted: 9 May 2016  
© Springer-Verlag Berlin Heidelberg 2016

**Abstract** Generation of concentration gradients of reactive molecules is of fundamental importance for many applications including biology, pharmaceutical and chemical engineering. By numerically simulating the flow behaviour, we reveal the possible factors that cause significant error in the gradients generated by the conventional universal microfluidic gradient generator (MGG) device reported previously. Based on these computational analyses, we optimize the geometrical design of the conventional 2-inlet MGG devices and improve the accuracy of the generated gradients. Moreover, we innovatively propose a 3-inlet MGG design showing desirable accuracy and versatility on creating various gradient profiles using the one single device. We further demonstrate our numerical simulation by fabricating the MGG devices by soft lithography and experimentally produce concentration gradients of diverse power functions. In general, the current study substantially improves the performance of universal MGG devices, which can serve as powerful tools for widespread applications in biology and chemistry.

**Keywords** Microfluidics · Concentration gradient generator · Nonlinear gradients · Flow-based

## 1 Introduction

The preparation of concentration gradients of reactive molecules is fundamentally important for many research fields including biology, pharmaceutical and chemical engineering (Kim et al. 2010; Lin and Levchenko 2015; Sackmann et al. 2014; Sant et al. 2010; Wu et al. 2010). To generate concentration gradients, microfluidic gradient generators (MGGs), including flow based and (Abe et al. 2015; Chen et al. 2012; Friedrich et al. 2012; Lin et al. 2004; Wang et al. 2015; Yang et al. 2011) diffusion based (Brett et al. 2012; Saadi et al. 2007; Sahai et al. 2011), and active MGGs (Ahmed et al. 2013; Destgeer et al. 2014; Jain et al. 2010) have recently emerged as a powerful tool to produce the desired concentration gradients in a controlled manner. Among these studies, a flow-based “universal MGG”, which is able to produce arbitrary monotonic gradients from two input concentrations, has attracted considerable attention (Irimia et al. 2006). Compared to other flow-based MGG devices such as “Christmas tree” (Lin et al. 2004) and radical-structured (Wang et al. 2015) designs which need to design separate channels to control the flows, universal MGG only needs to place a set of flow dividers along the flow direction in one single channel, so as to split and remix the flows of different concentrations. Such strategy to manipulate the flow behaviour renders universal MGG devices simple and cost efficient. Recently, increasing numbers of experimental researches (Xu et al. 2012) and numerical simulations (Hu et al. 2011) have been conducted on design and applications of universal MGGs, which have shown agreement with the original

**Electronic supplementary material** The online version of this article (doi:10.1007/s10404-016-1749-7) contains supplementary material, which is available to authorized users.

✉ Pengfei Wang  
peng@zju.edu.cn

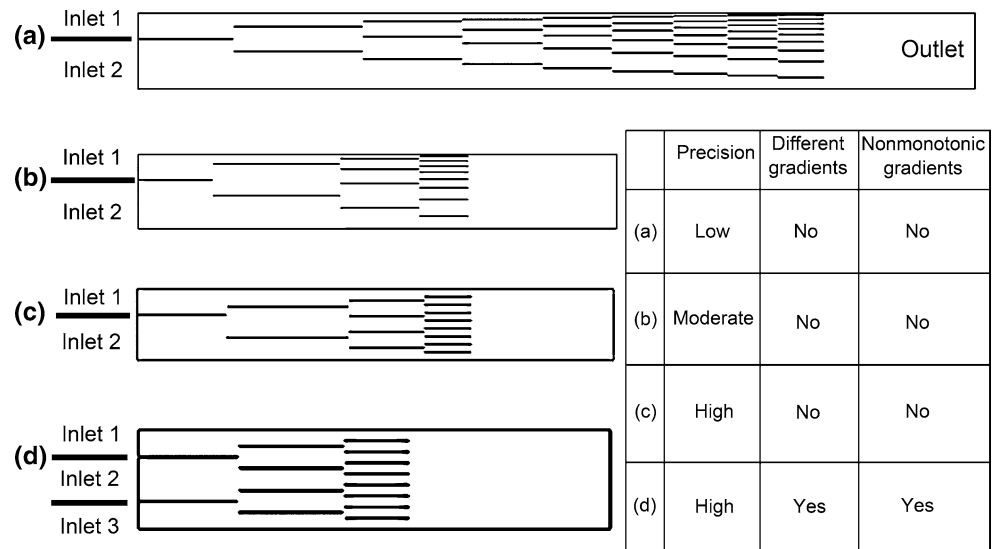
✉ Huanan Wang  
huananwang@dlut.edu.cn

<sup>1</sup> College of Chemical and Biological Engineering, Zhejiang University, Hangzhou 310027, People's Republic of China

<sup>2</sup> John A. Paulson School of Engineering and Applied Sciences, Harvard University, Cambridge, MA 02138, USA

<sup>3</sup> School of Life Science and Biotechnology, Dalian University of Technology, Dalian 116023, People's Republic of China

**Fig. 1** **a** Geometric model abstracted from the conventional 2-inlet MGG design. The grids are locally refined near the walls during meshing. **b** Geometric model of the optimized 2-inlet MGG design with reduced levels of dividers compared to (a). **c** Geometric model of optimized 2-inlet MGG design with reduced levels of dividers based on a new approximation method for the target function in comparison with the literature. **d** Geometric model of the novel 3-inlet MGG design. Comparisons between these geometries are shown in a chart



work. However, these studies only demonstrated the effectiveness of conventional MGG devices in generating linear concentration gradients. While it remains unclear whether these MGG devices work effectively for nonlinear gradients, and this might be of special interest for certain applications (Ahmed et al. 2010). Moreover, according to the previous report (Irimia et al. 2006), the efficiency of conventional universal MGG design is rather low; especially, each specific MGG design can only generate one gradient profile, which makes it not applicable for applications where dynamic changes of concentration gradients are needed (Atencia et al. 2012). Therefore, it remains a challenge to design a versatile and cost-efficient MGG device that is capable of producing concentration gradients in a more precise and controlled manner.

Here, we report a new generation of universal MGG devices based on numerical simulation of the flow behaviour within the microchannels. We reveal the existing problems in conventional MGG design that cause significant error in the resulting concentration gradients in experiments. We find that the error is primarily caused by the “wall effect” and unexpected diffusion between parallel channels. According to the numerical results, we further propose an optimized 2-inlet MGG design, which shows significantly improved precision in the resultant gradient profile compared to the conventional design. Furthermore, we innovatively develop a MGG device with three independent input concentrations. Such design allows creating concentration gradients with diverse functions using the same device. To further demonstrate the conclusion from numerical simulation, we test the proposed MGG designs experimentally by fabricating MGG devices by soft lithography (Xia and Whitesides 1998). The experimental results confirm our analysis; especially, by using one single 3-inlet MGG device, we achieve concentration gradients of

various power functions in a simple and efficient way and enable the production of dynamic concentration profiles.

## 2 Geometry and algorithm

### 2.1 Geometry and algorithm in conventional MGG

We first optimize the universal MGG design by Irimia et al. (2006) by analysing the methodology that was used and then numerically simulating the flow behaviour to elucidate the potential factors that cause error. The geometric model of the conventional 2-inlet MGG with nine-level flow dividers is replicated according to the previous study by Irimia et al. (2006), which aims to generate exponential gradient  $y = (e^{2x} - 1)/(e^2 - 1)$ . The geometry of the microchannel is shown in Fig. 1a. The width of the main channel is set to 400  $\mu\text{m}$  and the width of the dividers to 2  $\mu\text{m}$ . The location of flow dividers within the channel remains the same as the previous study (Irimia et al. 2006), but the length of the dividers at the downstream levels is elongated to ensure sufficient diffusion and complete mixing of two adjacent streams of different concentrations. Considering the significantly smaller dimension of the height of the microchannel compared to the width and length, hereby we consider the 3D microfluidic MGG devices as a 2D geometric model to simplify the simulation without introducing significant error.

In previous design by Irimia et al. (2006), each individual stream (except the ones close to the walls) is split by the flow divider and remixed downstream with its two adjacent streams to generate two new concentrations (Fig. 2a). According to the mass conservation equation, concentrations and geometric parameters are related as follows:

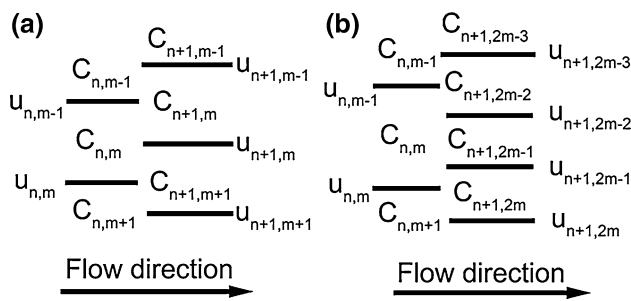


**Fig. 2** Algorithm method for fluid distribution in **a** the conventional gradient generator and **b** the optimized fluid distribution

$$C_{n+1,m} \cdot (u_{n+1,m} - u_{n+1,m-1}) = C_{n,m-1} \cdot (u_{n,m-1} - u_{n+1,m-1}) + C_{n,m} \cdot (u_{n+1,m} - u_{n,m-1}) \tag{1}$$

where  $C_{i,j}$  denotes the concentration at channel  $j$  in level  $i$  and  $u_{i,j}$  denotes the positions of divider  $j$  with respect to the side of the main channel at level  $i$ .

### 2.2 Optimization of the geometry and algorithm

In conventional MGG devices designed by Irimia et al. (2006), two significant factors have been neglected, which, however, play critical role in determining the resulting gradients in practice, that is (1) the unexpected diffusion that occurs at the transition site between two sequential levels of flow and (2) the “wall effect” resulting from the friction between fluids and the surfaces of microchannels. Both factors can lead to significant error in the output gradients. To address these problematic issues, we further optimize the geometry of MGG design.

According to our simulation, unexpected diffusion between different streams at the transition site between two sequential levels of flow dividers is very difficult to avoid. Therefore, our strategy is to reduce the levels of dividers without compromising the resolution of the gradient profiles. To this end, we first increase the numbers of dividers in each level; this allows to divide each individual stream into three instead of two streams in the previous MGG designs (Fig. 2b). This also changes the relationship between concentrations of each stream and the positions of the dividers:

$$C_{n+1,2m-2} \cdot (u_{n+1,2m-2} - u_{n+1,2m-3}) = C_{n,m-1} \cdot (u_{n,m-1} - u_{n+1,2m-3}) + C_{n,m} \cdot (u_{n+1,2m-2} - u_{n,m-1}) \tag{2}$$

and

$$C_{n,m} = C_{n+1,2m-1} \tag{3}$$

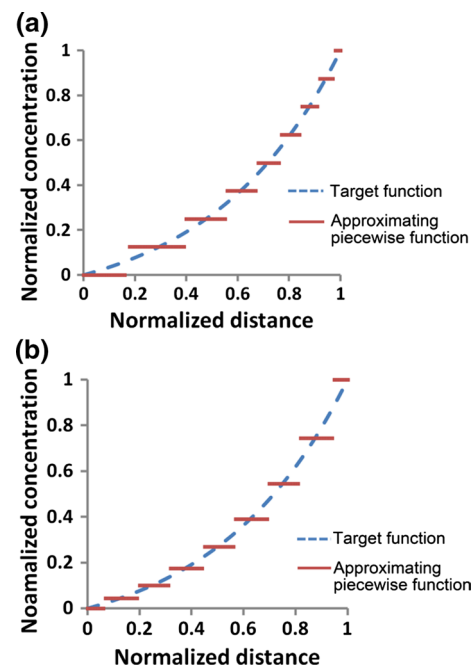


**Fig. 3** Comparison between the target function gradient (dashed line) and the piecewise approximating function (dense line) at the eighth level. **a** Approximation method used in conventional gradient generator. **b** Optimized approximation method

As a result, the number of dividers in each level increases in an exponential manner along the flow direction (Fig. 1b), rather than in a linear manner as in the conventional MGG design (Fig. 1a). We find that such a simple modification substantially enhances the efficiency of concentration distribution based on our simulation. Moreover, we can achieve target gradient using considerably reduced levels of dividers, thereby facilitating less diffusion at the transition site.

To reduce the nonuniform flow caused by the wall effect, we further optimize the approximation method of the output gradients. To create an output gradient approaching the target gradient, we normally consider the target concentration as a piecewise function profile. The conventional universal MGGs typically adopt the mathematically optimal approximation method, in which the spacing of dividers decreases as the slope of the target gradient increases (Fig. 3a). Such method leads to nonuniform spacing between flow dividers and consequently results in differences in the flow rate between each stream. This directly causes considerable error in the resulting concentration gradients using conventional MGG devices. To address this issue, we improve the approximation method from Irimia et al. (2006) by transferring the target profile into a piecewise function with constant distance (Fig. 3b), thus reducing the flow rate differences to the maximum extent. This means the spacing

between dividers is almost constant in most of the levels regardless the slope of the target gradient.

After determining the piecewise concentration distribution of the output gradient profiles and the positioning of the flow dividers in the last level, we further computationally calculate the geometric design of upstream by Eqs. (2) and (3). Besides, the length of the dividers can be calculated based on the diffusion time of certain molecules:  $t = l/v$  and  $t \sim w^2/D$ , where  $l$  is the length of the dividers,  $w$  is the maximum spacing between the dividers in the same level,  $v$  is the flow velocity and  $D$  is the diffusion coefficient. By modifying the algorithm given by Irimia et al. (2006), we propose a new method (see Fig. S1 in Online Resource 1) which takes into account both above-mentioned factors that cause the error. As shown in Fig. 1c, the geometric design after our optimization exhibits an almost uniform distribution of flow dividers.

Furthermore, another drawback of the conventional 2-inlet MGG devices is their incapability to generate diverse gradient profiles using the one single geometry. Therefore, we hereby propose a novel 3-inlet MGG; this new design allows to produce concentration gradients of different power function using exactly the same device (as shown in Fig. 1d). The three input fluids are completely independent to each other, hence allowing for tailoring either the velocity or the concentration of input solutions to achieve desirable gradient or dynamic change of local concentration within the microchannel.

### 3 Simulation method and experimental settings

#### 3.1 Simulation method

Because the positioning of the dividers is rather complex and the status of the flow field cannot be correctly acquired based on the previous method (Dertinger et al. 2001; Toh et al. 2014), hereby we simulate the flow behaviour within microchannel of different geometry. The simulation was conducted by a commercial computational fluid dynamics software FLUENT, which is based on finite-volume method. The species transport and laminar flow model were adopted to solve these convection–diffusion problems. Steady pressure-based solver and Semi-Implicit Method for Pressure Linked Equations-Consistent (SIMPLEC) were used. The values of the pressure-correction under-relaxation factor were by default, specifically 0.3 for pressure, 0.7 for momentum and 1 for density, body forces and diffusion. The third-order MUSCL was used for spatial discretization of momentum and diffusion. The discretization of the gradient and pressure was, respectively, the Green–Gauss node-based and the standard method. The residuals were all set as  $1 \times 10^{-7}$ . The geometric models

were meshed by the software Gambit, and the grids were locally refined near the walls. If no other status was given, the parameters of the fluid were set to those of water, with a diffusion coefficient of  $4.2 \times 10^{-10} \text{ m}^2/\text{s}$  referring to that of fluorescein dye (Culbertson et al. 2002). The flow rate at the input was set as  $2 \times 10^{-5} \text{ m/s}$ , and the pressure of the outlet was set as 0 gauge pressure. The initial concentrations of the two input streams were, respectively, 0 and 1. In the 3-inlet MGG, the velocity of inlet 2 was set to  $2 \times 10^{-5} \text{ m/s}$ , and the concentration of it was calculated to be the target function value at the middle point in the perpendicular direction, while the concentrations of inlet 1 and inlet 3 were, respectively, 1 and 0. The concentration data at  $25 \mu\text{m}$  downstream from the outlet of the last level of dividers were taken as the final gradient.

#### 3.2 Preparation of MGG devices

Experiments were further conducted to test the accuracy of our simulation. MGG devices with proposed 2-inlet and 3-inlet MGG designs (see Fig. S2 in Online Resource 1) were fabricated by soft lithography using poly(dimethylsiloxane) (PDMS) following a protocol reported recently (Mazutis et al. 2013). Microchannels with a width of 1.6 mm and a height of  $30 \mu\text{m}$  were used as a result of the limitations of our experimental set-up. The experimental details of fabrication of PDMS with patterned microchannels are shown in the Online Resource 1. The PDMS was then treated with oxygen plasma and bounded to the clean glass slice. To prevent the air bubbles to adhere on the inner walls of the device, which could cause significant error in resultant gradients, the originally hydrophobic PDMS microchannels were treated with hydrophilic polyelectrolytes. Briefly, ionic [poly(sodium 4-styrenesulfonate) and cationic poly(diallyldimethylammonium chloride)] aqueous solutions were alternately injected into the microchannel for at least three cycles, followed by washing with distilled water for three times.

#### 3.3 Microfluidic device operation

Aqueous solutions with various concentrations of fluorescein sodium salt were prepared as the starting fluids. For the 2-inlet MGG, based on our simulation, a fluorescein solution with a concentration of 5 mg/L was input into inlet 1 at a flow rate of 20.16 nL/min, and distilled water was input into inlet 2 at a flow rate of 35.88 nL/min. For the 3-inlet MGG, 5 mg/L fluorescein solution and distilled water were input into inlets 1 and 3, respectively. Another fluorescein solution with various concentrations depending on the target gradients (the concentrations are listed in Table 1) was input into inlet 2. The flow rate of inlet 2 was kept constant at 24.16 nL/min, while the flow rates for

**Table 1** Flow rates of inlet 1 and inlet 3 and the concentration of fluorescein solution in inlet 2

| Target gradient | Flow rate of inlet 1 (nL/min) | Flow rate of inlet 3 (nL/min) | Concentration in the inlet 2 (mg/L) |
|-----------------|-------------------------------|-------------------------------|-------------------------------------|
| $y = x$         | 15.28                         | 15.28                         | 2.5                                 |
| $y = x^2$       | 9.17                          | 21.39                         | 1.25                                |
| $y = x^3$       | 7.64                          | 22.92                         | 0.625                               |
| $y = x^5$       | 4.58                          | 25.98                         | 0.156                               |
| $y = x^{0.5}$   | 9.93                          | 5.35                          | 3.55                                |
| $y = x^{0.33}$  | 9.17                          | 3.05                          | 3.95                                |

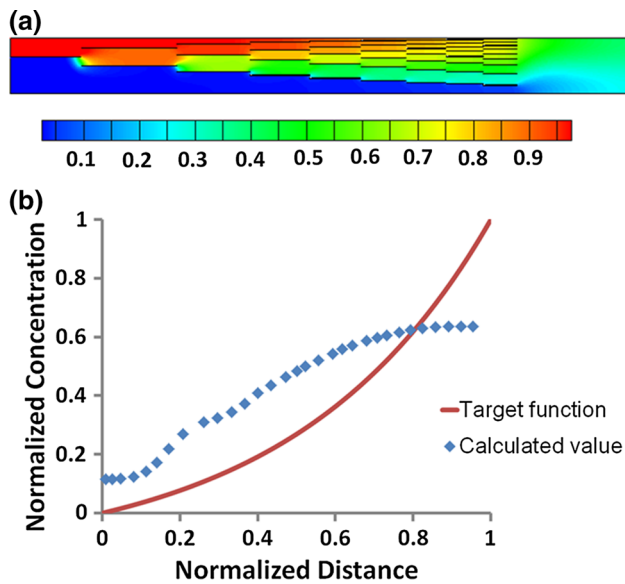


**Fig. 4** **a** Simulated mapping of the concentration distribution in the conventional exponential gradient generator. **b** Comparison between target concentration gradient (*dense line*) and calculated gradient profile (*diamond*) using the conventional gradient generator

inlets 1 and 3 are listed in Table 1. The concentration data were collected by imaging the fluorescein signals within the microfluidic device using a fluorescent microscope (Leica TCS SP5). The distribution of fluorescein molecules perpendicular to the flow direction at 100 μm downstream from the outlet of the last level of dividers was measured using software Leica LAS AF lite. Adjacent 10–15 data were averaged with respect to both location and concentration to reduce errors.

## 4 Results and discussion

### 4.1 Error analysis of conventional 2-inlet universal MGG

Based on our simulation, we observe rather poor agreement between the resulting concentration gradient and

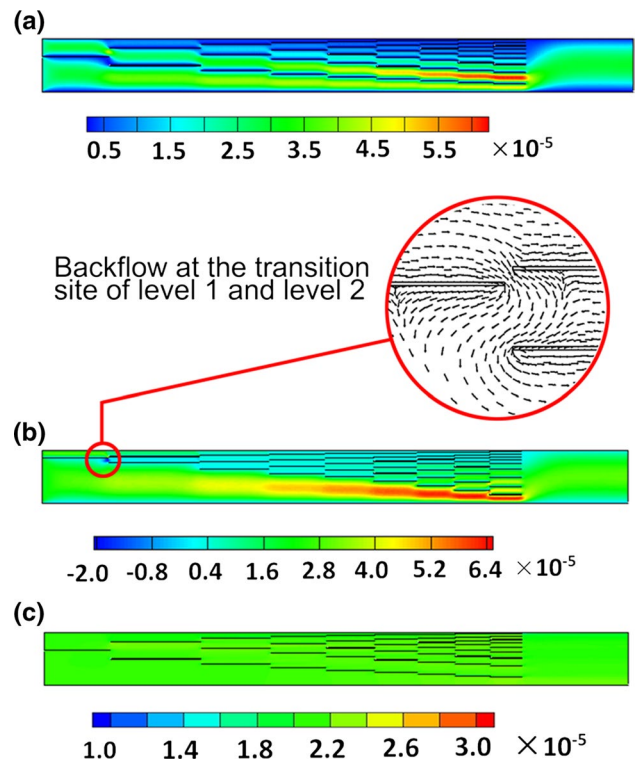


**Fig. 5** Simulated mapping of the flow velocity along the flow direction in the conventional MGG for generation of gradient of **a** exponential function and **b**  $y = x^5$  function with the viscosity of  $1 \times 10^{-3}$  Ns/m<sup>2</sup>; **c** gradient of exponential function with the viscosity of  $1 \times 10^{-20}$  Ns/m<sup>2</sup>. The vector *graph* is enlarged to show the vector profile and location of backflow

the targeting gradient using the previously reported universal MGG design by Irimia et al. (as shown in Fig. 4). The simulation confirms that the wall effect and the unexpected diffusion are the main reasons to cause the error. We further simulate velocity mapping throughout the microchannel, which reveals that the flow rate is nonuniform, as shown in Fig. 5a. This result indicates that the hypothesis of Irimia et al. (2006), where the flow rate was assumed to be consistent throughout the whole device, is fundamentally incorrect. Actually, the flow velocity is significantly higher when the spacing between adjacent dividers is larger (Fig. 5a). Additionally, we observe

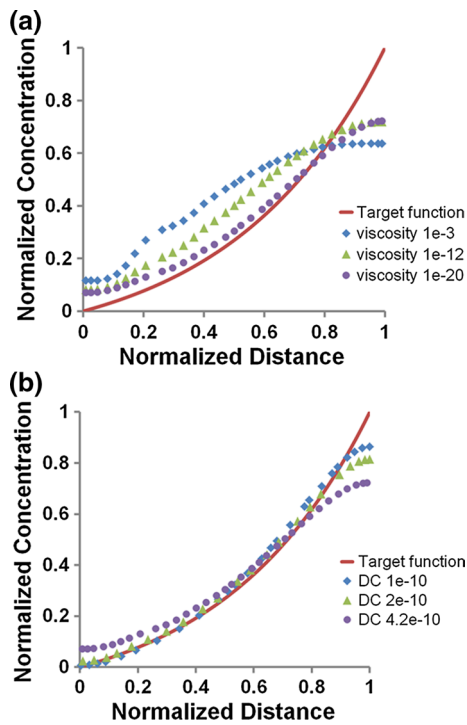


**Fig. 6** Comparison between target gradient (*dense line*) and simulated gradient profiles produced by conventional MGG using fluids of **a** different viscosities of  $1 \times 10^{-20}$  Ns/m<sup>2</sup> (*circle*),  $1 \times 10^{-13}$  Ns/m<sup>2</sup> (*triangle*) and  $1 \times 10^{-3}$  Ns/m<sup>2</sup> (*diamond*) (given the diffusion coefficient of  $4.2 \times 10^{-10}$  m<sup>2</sup>/s) and **b** different diffusion coefficients (DC) of  $1 \times 10^{-10}$  m<sup>2</sup>/s (*diamond*),  $2 \times 10^{-10}$  m<sup>2</sup>/s (*triangle*) and  $4.2 \times 10^{-10}$  m<sup>2</sup>/s (*circle*) (given a fluid viscosity of  $1 \times 10^{-20}$  Ns/m<sup>2</sup>)

backflow at the transition area between level 1 and level 2 in  $y = x^5$  function MGG (Fig. 5b). The nonuniform flow can be attributed to the wall effect of the flow dividers. In the region where dividers are closely positioned, the area of solid wall is larger, and the viscous resistance of flow is more prominent, as opposed to the smaller resistance existing in the other areas. This nonuniformity of the flow resistance consequently leads to the nonuniform flow and even backflow. As a result, the allocation of flow does not agree with the design, and a concentration error is introduced.

To prove this, we further conduct the simulation by changing the fluid viscosity and compare the simulated gradient profiles with the target one. The obtained concentration gradients show better agreement with the target one at a lower viscosity of  $1 \times 10^{-20}$  Ns/m<sup>2</sup>, as shown in Fig. 6a. This can be attributed to the uniform flow in the MGG at such low viscosity (Fig. 5c). However, accuracy of the resultant gradients decreases as the fluid viscosity increases. Moreover, this trend is independent to the target function of gradients (see Fig. S3 in Online Resource 1). Particularly, the backflow disappears as the viscosity decreases to lower than  $1 \times 10^{-12}$  Ns/m<sup>2</sup>, since the

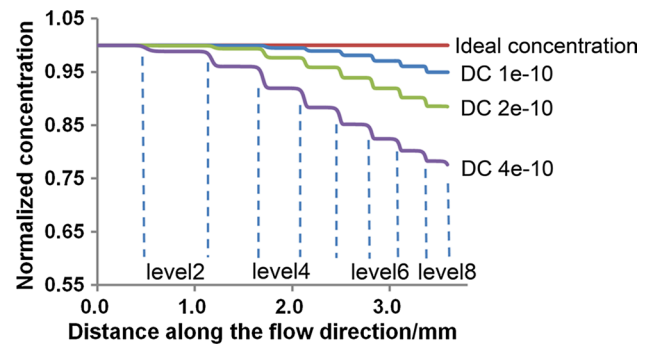


**Fig. 7** Concentrations at the wall of the main channel along the flow direction as a function of diffusion coefficients (DC)

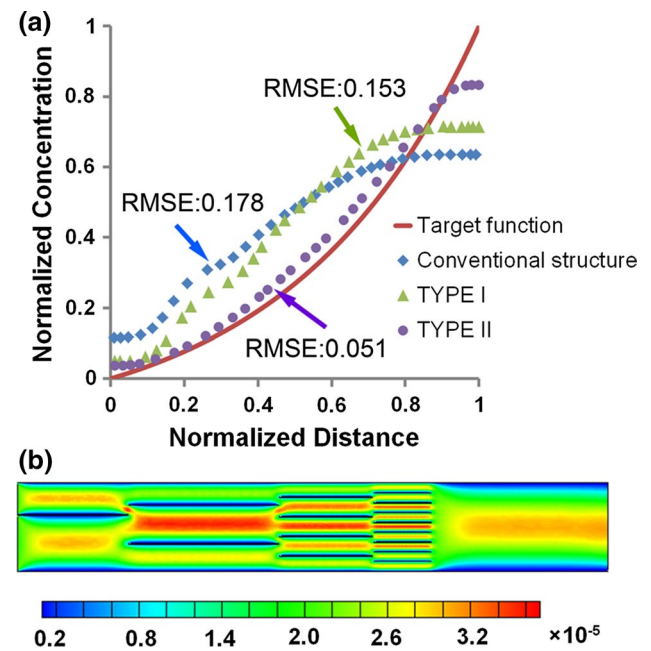


**Fig. 8** **a** Simulated concentration gradients produced by conventional MGG design (*diamond*), optimized MGG design of type I (*triangle*) and type II (*circle*). **b** Simulated mapping of flow velocities in the optimized MGG design of type II

resistance difference caused by the wall effect is not enough to create a backflow. Based on the fact that the backflows occur in the gradient of  $y = x^5$  function instead of the exponential function and at the viscosity of  $1 \times 10^{-3}$  Ns/m<sup>2</sup> instead of  $1 \times 10^{-20}$  Ns/m<sup>2</sup>, we can conclude that the form of backflow is determined by the target gradient and the viscosity of the fluid. To generate target gradient with very steep slope, the spacing of adjacent dividers has to be decreased locally, which can create higher resistance difference. On the other hand, for the same target gradient, higher viscosity may induce the backflow according to Newton’s law of viscosity. Based on the above analysis, since the viscosity of the fluid normally cannot be changed,

the local spacing between dividers should not be too small so as to prevent the backflow.

In addition to the effect of nonuniform flow rate, diffusion between adjacent streams at the transition site between two levels of dividers could also lead to deviation from the target concentrations. To prove this, we simulate the evolution of molecule concentration at the wall site as passing nine levels of dividers. Ideally, the concentration at the wall site should remain to be 1, if no diffusion occurs at the transition sites between levels. However, we observe that the resulting concentration significantly decreases upon passing each transition sites. Such decrease in concentration becomes more obvious as the diffusion coefficient increasing from  $1 \times 10^{-10}$  to  $4.2 \times 10^{-10} \text{ m}^2/\text{s}$ , as shown in Fig. 7. More importantly, such diffusion not only happens at the vicinity of the wall, but also at other transition site between levels of dividers; therefore, the resultant gradient profiles show increasing error at higher diffusion coefficient (Fig. 6b).

### 4.2 Optimization of the 2-inlet universal MGG

To optimize the performance of conventional 2-inlet universal MGG, we modify the previous design by reducing the levels of dividers (Fig. 1b, denoted as type I design) and further changing the approximation method (Fig. 1c, denoted as type II design). We further compare our modified design with the conventional one, as shown in Fig. 8a. The parameters of fluid properties are kept consistent with the experimental set-up, that is the viscosity of  $1 \times 10^{-3} \text{ Ns/m}^2$  (the same to water) and diffusion coefficient of  $4.2 \times 10^{-10} \text{ m}^2/\text{s}$  (the same to fluorescein molecule). Apparently, the modified MGG designs display a significantly up-regulated correlation with the target gradient than those of the conventional MGG design, as evidenced by the much lower root-mean-square error (RMSE, see Online Resource 1 for detail) values of type I and type II MGG designs. The gradient produced by type I MGG shows a RMSE value of 0.153 instead of the value 0.178 of conventional design, which confirms our theory that reducing the levels of dividers significantly diminishes the effect of diffusion at each transition sites between levels. The RMSE value of the gradient produced by the type II design decreases to 0.051, which confirms the positive effects of changing the approximation method. Moreover, the flow velocities in the flow field of the proposed type II MGG are also simulated, as shown in Fig. 8b. The overall velocities are almost homogeneous throughout the device, confirming that the optimized design is more applicable to the mass conservation equation of Eqs. (1) and (2). This also indicates that the optimization method is effective for MGGs of different gradients. Despite the wall effect and the unexpected diffusion are different according to different

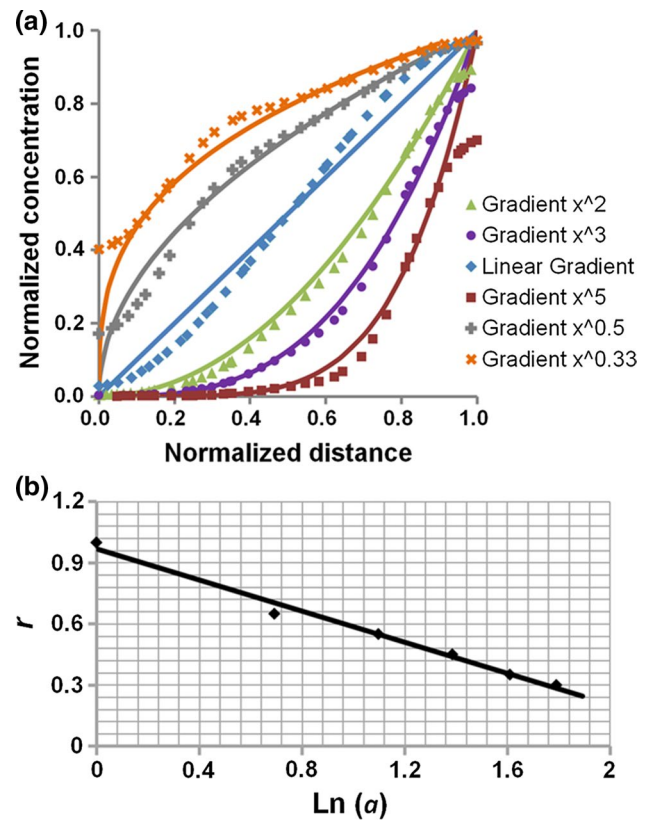


**Fig. 9** a Simulated concentration gradients of different power functions (dots) using a 3-inlet MGG compared with the target gradient profiles (dense lines). b The relationship between the power  $a$  in the function  $y = x^a$  ( $a \geq 1$ ) and the velocity ratio  $r$  of inlet 1 and inlet 2

designs, they play less important roles in affecting the accuracy of the concentration gradients in the optimized geometries we proposed hereby. According to the above discussion, when the target gradient is linear, which means the dividers are placed uniformly in the device geometry, the error of the gradient is small. That is why no significant error was observed and noticed by Xu et al. (2012) and Hu et al. (2011).

### 4.3 3-inlet MGG design

Because conventional 2-inlet MGG can only generate a single gradient profile using the same device, we propose a new design of 3-inlet MGGs based on the above-mentioned algorithm (Fig. 1d). This innovative design facilitates the production of gradients with various power functions using the same MGG device by tailoring the initial velocities and concentrations of each stream of three independent inlets. As shown in Fig. 9a, 3-inlet MGG devices provided a high extent of freedom in generating gradients with different power functions, which can serve as a simple and efficient platform for applications in generating concentration gradients; especially, we

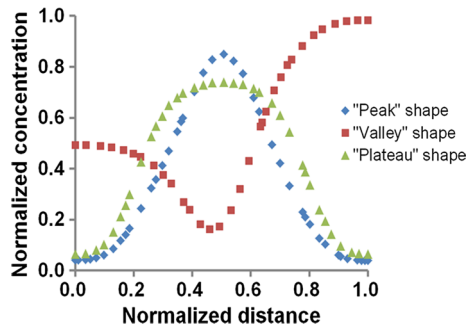


**Fig. 10** Simulated concentration gradients of “peak”, “valley” and “plateau” shape

find that the value of the power  $a$  in function  $y = x^a$  ( $a \geq 1$ ) shows a linear relationship with the velocity ratio  $r$  of inlet 1 and inlet 2 that  $r = 0.95 - 0.41\text{Ln}(a)$ , where  $\text{Ln}(a)$  denotes the natural logarithm of  $a$  (Fig. 9b). This relationship indicates that by a mathematical calculation of the inlet velocities based on the output target, user-defined gradients with various power functions can be generated. Furthermore, we demonstrate that nonmonotonic gradients can be achieved using 3-inlet MGGs based on numerical simulation. As shown in Fig. 10, by adjusting the velocity and concentration of each input stream, “peak”-, “valley”- and “plateau”-shaped concentration profiles can be produced.

These results demonstrate that the proposed 3-inlet MGGs exhibit superior properties in comparison with the conventional 2-inlet MGGs. First, 3-inlet designs are more cost-effective in preparing gradients, which are capable of producing gradients of different power function using the same geometry. Second, they are able to produce nonmonotonic gradients. Third, 3-inlet designs allow to adjust the gradients dynamically during the experiments. Furthermore, compared with other flow-based MGGs such as Christmas tree and radial types, the design of this 3-inlet MGG is much simpler. Compared with diffusion-based MGGs, the 3-inlet MGG is more suitable for generating nonlinear gradients and can provide microenvironments with shear stress. Meanwhile, no extra equipment and actuators are needed compared with active MGGs. Therefore, we expect our proposed MGGs can serve as a better tool for more biomedical and pharmaceutical applications considering the enhanced accuracy and versatility in comparison with conventional universal MGGs.

#### 4.4 Experimental results

The simulated gradient resulting from type II MGG is further demonstrated by experiment, which shows that the gradient profile generated using PDMS microfluidic devices correlates well with the target exponential gradient and simulated result. As shown in Fig. 11a and Fig. S4 (a)

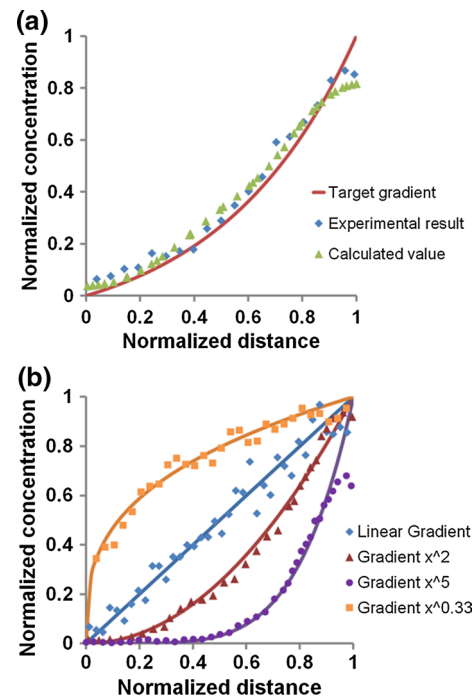


**Fig. 11** **a** Measured concentration gradient produced by the proposed type II 2-inlet MGG (*diamond*) compared with target exponential gradient (*dense line*) and the simulated result (*triangle*). **b** Measured concentration gradients with various power functions produced by the proposed 3-inlet MGG (*dots*) compared with the related target gradient profiles (*dense lines*). Representative gradient profiles with power function  $a < 1$ ,  $a = 1$ , and  $a > 1$  are shown

in Online Resource 1, a RMSE value of 0.058 is achieved, confirming the accuracy and efficiency of our analysis and simulation methods on conventional 2-inlet MGG devices. The simulation results of 3-inlet MGG are also validated by experiments. By using the same device, we successfully generate gradients of different power functions, that is,  $a = 1$ ,  $a > 1$ , or  $a < 1$ , which matches well with the theoretical target gradients (as shown in Fig. 11b, Figs. S4 (b) and S5 in Online Resource 1).

The deviations of gradient profiles from target profiles near the boundary area can be observed both in simulation and experimental results. Hence, it is considered to be a normal physical phenomenon. As can be seen from Fig. 4b, the slope of target exponential gradient profile is very steep near the boundary. According to the Fick’s law, the local diffusion in this area should be very quick due to the significant concentration difference. Thus, the profiles near the boundaries are hard to keep unchanged after the fluid leaves the last level of dividers.

#### 4.5 Operating conditions of the proposed MGGs

It needs to be pointed out that the proposed MGG designs are only valid for conditions where the diffusion dominates

convection within the microchannels. This can be referred to the Peclet number, which is the ratio of convection to diffusion, i.e.  $Pe = \frac{vL}{D}$ , where  $v$  is the flow velocity,  $D$  is the diffusion coefficient of the fluids,  $L = w^2/l$  is the characteristic length determined by the sizes of the MGGs ( $w$  and  $l$  are the width and length of the channel, respectively). Therefore, to allow the proposed MGGs to generate gradient with desirable accuracy, lower flow velocity and larger diffusion coefficient of the fluids are preferred, so as to result in  $Pe \leq 1$ . If the flow velocity is too high or the diffusion coefficient is too small, convection will dominate diffusion and result into significant errors in the resulting gradient profiles. Therefore, we use relatively low-flow rates in the current study. However, above analysis shows that such device allows functioning at various flow rates. To obtain the same target, gradient at higher flow rate requires to elongate the channels or to increase the diffusion coefficient to achieve complete mixing.

## 5 Conclusions

By numerically simulating the flow behaviour in conventional universal MGG device, we reveal the problems that cause considerable error in the resulting gradients prepared by conventional MGG design. Based on these analyses, we propose optimized MGG designs with enhanced accuracy and ability to create various types of gradient profiles using the same device, which are demonstrated by simulation. Experiments are further performed to confirm our simulation using MGG devices made of PDMS. In general, based on analysis of convection and diffusion of microflows, we improve and develop a class of MGG device used to generate concentration gradients of desirable molecules, which can serve as a better tool for more biomedical and pharmaceutical applications considering the enhanced accuracy and versatility in comparison with conventional universal MGGs.

The focus of this current study is to use numerical simulation to analyse and improve the long-existing problematic issues in the conventional 2-inlet MGGs. The 3-inlet system is of more interest and worth to getting more detailed analysis, but this is also out of the scope of the current study. Actually, we are currently study more in details of the 3-inlet MGG devices, the results of which will be reported later in our work.

**Acknowledgments** This work was supported by the National Natural Science Foundation of China (Nos. 51373153 and 51503208), National Basic Research Program of China (Grant No. 2015CB057301), the Fundamental Research Funds for the Central Universities of China (No. DUT15RC(3)113), the National Science Foundation (DMR-1310266) and the Harvard Materials Research Science and Engineering Center (DMR-1420570).

## Compliance with ethical standards

**Conflict of interest** The authors declare that they have no conflict of interest.

## References

- Abe Y, Kamiya K, Osaki T, Sasaki H, Kawano R, Miki N, Takeuchi S (2015) Nonlinear concentration gradients regulated by the width of channels for observation of half maximal inhibitory concentration (IC 50) of transporter proteins. *Analyst* 140:5557–5562
- Ahmed T, Shimizu TS, Stocker R (2010) Bacterial chemotaxis in linear and nonlinear steady microfluidic gradients. *Nano Lett* 10:3379–3385
- Ahmed D, Chan CY, Lin SCS, Muddana HS, Nama N, Benkovic SJ, Huang TJ (2013) Tunable, pulsatile chemical gradient generation via acoustically driven oscillating bubbles. *Lab Chip* 13:328–331
- Atencia J, Cooksey GA, Locascio LE (2012) A robust diffusion-based gradient generator for dynamic cell assays. *Lab Chip* 12:309–316
- Brett ME, DeFlorio R, Stone DE, Eddington DT (2012) A microfluidic device that forms and redirects pheromone gradients to study chemotropism in yeast. *Lab Chip* 12:3127–3134
- Chen CY, Wo AM, Jong DS (2012) A microfluidic concentration generator for dose-response assays on ion channel pharmacology. *Lab Chip* 12:794–801
- Culbertson CT, Jacobson SC, Ramsey JM (2002) Diffusion coefficient measurements in microfluidic devices. *Talanta* 56:365–373
- Dertinger SKW, Chiu DT, Jeon NL, Whitesides GM (2001) Generation of gradients having complex shapes using microfluidic networks. *Anal Chem* 73:1240–1246
- Destgeer G, Im S, Ha BH, Jung JH, Ansari MA, Sung HJ (2014) Adjustable, rapidly switching microfluidic gradient generation using focused travelling surface acoustic waves. *Appl Phys Lett* 104:023506
- Friedrich D, Please CP, Melvin T (2012) Design of novel microfluidic concentration gradient generators suitable for linear and exponential concentration ranges. *Chem Eng J* 193:296–303
- Hu Y, Zhang X, Wang W (2011) Simulation of the generation of solution gradients in microfluidic systems using the lattice Boltzmann method. *Ind Eng Chem Res* 50:13932–13939
- Irimia D, Geba DA, Toner M (2006) Universal microfluidic gradient generator. *Anal Chem* 78:3472–3477
- Jain M, Yeung A, Nandakumar K (2010) Induced charge electro-osmotic concentration gradient generator. *Biomicrofluidics* 4:014110
- Kim S, Kim HJ, Jeon NL (2010) Biological applications of microfluidic gradient devices. *Integr Biol* 2:584–603
- Lin B, Levchenko A (2015) Spatial manipulation with microfluidics. *Front Bioeng Biotechnol* 3:39
- Lin F, Saadi W, Rhee SW, Wang SJ, Mittal S, Jeon NL (2004) Generation of dynamic temporal and spatial concentration gradients using microfluidic devices. *Lab Chip* 4:164–167
- Mazutis L, Gilbert J, Ung WL, Weitz DA, Griffiths AD, Heyman JA (2013) Single-cell analysis and sorting using droplet-based microfluidics. *Nat Protoc* 8:870–891
- Saadi W, Rhee SW, Lin F, Vahidi B, Chung BG, Jeon NL (2007) Generation of stable concentration gradients in 2D and 3D environments using a microfluidic ladder chamber. *Biomed Microdevices* 9:627–635
- Sackmann EK, Fulton AL, Beebe DJ (2014) The present and future role of microfluidics in biomedical research. *Nature* 507:181–189
- Sahai R, Cecchini M, Klingauf M, Ferrari A, Martino C, Castrataro P, Lionetti V, Menciassi A, Beltram F (2011) Microfluidic chip for

- spatially and temporally controlled biochemical gradient generation in standard cell-culture Petri dishes. *Microfluid Nanofluid* 11:763–771
- Sant S, Hancock MJ, Donnelly JP, Iyer D, Khademhosseini A (2010) Biomimetic gradient hydrogels for tissue engineering. *Can J Chem Eng* 88:899–911
- Toh AGG, Wang ZP, Yang C, Nguyen NT (2014) Engineering microfluidic concentration gradient generators for biological applications. *Microfluid Nanofluid* 16:1–18
- Wang H, Chen CH, Xiang Z, Wang M, Lee C (2015) A convection-driven long-range linear gradient generator with dynamic control. *Lab Chip* 15:1445–1450
- Wu MH, Huang SB, Lee GB (2010) Microfluidic cell culture systems for drug research. *Lab Chip* 10:939–956
- Xia Y, Whitesides GM (1998) Soft lithography. *Annu Rev Mater Sci* 28:153–184
- Xu C, Poh YKC, Roes I, O’Cearbhaill ED, Matthiesen ME, Mu L, Seung YY, Nieves DM, Irimia D, Karp JM (2012) A portable chemotaxis platform for short and long term analysis. *PLoS one* 7:e44995
- Yang CG, Wu YF, Xu ZR, Wang JH (2011) A radial microfluidic concentration gradient generator with high-density channels for cell apoptosis assay. *Lab Chip* 11:3305–3312